Closed-Form Spectral Computation of Intermodulation Distortion for Shunt-Based Current Measurements

PELLE WEILER[1] **(Graduate Student Member, IEEE), BAS VERMULST**[1] **(Member, IEEE),
ERIK LEMMEN**[1]**, AND KORNEEL WIJNANDS**[2] **(Member, IEEE)**

[1]Electromechanics and Power Electronics Group, Eindhoven University of Technology, 5600 MB Eindhoven, The Netherlands

[2]Electrical Energy Systems Group, Eindhoven University of Technology, 5600 MB Eindhoven, The Netherlands

CORRESPONDING AUTHOR: P. WEILER (e-mail: b.p.weiler@tue.nl)

ABSTRACT This work presents a closed-form analytic approach to calculate the distortion introduced in resistive current measurements due to thermal properties of shunt resistors. As a shunt's resistance varies with temperature, the sensed voltage becomes distorted. This non-linear effect depends on the thermal interface, dissipated power and material properties of the shunt resistor. It is presented, how to simplify the non-linear equation of the shunt temperature and calculate the resulting voltage spectrum, without the use of computationally extensive time-to-frequency-domain transforms. The results of the presented method match simulations including the non-linear behaviour, enabling a quick search through a solution space. The method is experimentally verified by use of a linear amplifier with an output distortion of −90 dB at low frequencies. In the experiment, a total harmonic distortion of up to −70 dB is observed in several shunt resistors covering a range of different thermal properties. Based on the presented method, shunt resistors can be chosen according to the minimum distortion required in a given application. Depending on the frequencies of interest, shunt resistors with a high temperature coefficient might still offer sufficient distortion performance.

INDEX TERMS Current measurement, high-precision, intermodulation distortion, self heating, shunt resistor, total harmonic distortion.

I. INTRODUCTION

COMPARED to other current-sensing methods, resistive shunt elements can offer high precision and bandwidth [1]. Both aspects are required in high-precision applications, where output powers of several kilowatts are regulated to a precision of microamperes within milliseconds [2], [3]. The power amplifiers delivering this current are optimized for high bandwidth and low distortion. The total output distortion is a combination of several factors, such as the dead-time and modulation of the amplifier [4]. Most of these aspects can be mitigated by changes in amplifier topology or compensation structures in the amplifier's control [5], [6]. However, for low frequencies the most significant reduction in distortion comes from feedback control of the amplifier's output, as the control loop is able to

suppress errors below the controllers bandwidth. This feedback relies on a precise measurement of the output current, since any measurement error is falsely interpreted as output error. In case of feedback with a shunt resistor, the shunt's output voltage will contain errors depending on the amplitude and frequency of the measured current, next to other environmental factors [7], [8].

A shunt resistor's output voltage is the product of the sensed current and the resistance, which should create an ideal linear sensor. However, due to material properties, the resistance varies with temperature [9]. This temperature dependence creates an error in the output voltage. In the field of microwave electronics, this effect is referred to as intermodulation distortion due to self-heating, which can occur in both passive and active circuit

components [10], [11]. The same mechanism results in distortion on a resistor. Audio applications encounter this distortion when using resistors in feedback circuits, where they add unwanted spectral components [12]. This effect has been demonstrated in [13]. The source of the distortion is the varying power dissipation in the resistor, caused by the sensing current. As the power dissipation is proportional to the square of the current, the shunts temperature will experience two extrema in one period, and so does its resistance due to the temperature dependence. For sinusoidal currents, this varying resistance results in an output voltage containing harmonics of the measured signal. The magnitude of these harmonics can be reduced by selecting a shunt with a lower temperature coefficient of resistance (TCR). Modern shunt elements offer TCRs of less than 5 ppm, which is more than sufficient to reach a total harmonic distortion (THD) below -120 dB [14], [15]. However, component cost can also be a driving factor, which encourages the use of cheaper resistors with larger TCR.

Selection of the right shunt resistor then becomes a trade-off between obtainable precision, ability of compensation and cost. Given the application requirements, simple distortion approximations can be made by considering the power dissipation caused by the nominal shunt resistance and input current. For more precise results, time-based simulation including the temperature dependence can be done, followed by a Fourier transform to obtain the shunt's voltage spectrum [16].

The goal of this work is to quantify the effect of intermodulation distortion, including the quadratic temperature dependence of the shunt, in a closed-form solution as opposed to iterative simulation. In this paper, a solution is presented, which yields the third and fifth harmonic of the shunt voltage and does not rely on time-based simulation. First, the discrete Fourier series of the shunt's temperature is calculated, unaffected by self-heating. Then, assuming quadratic temperature dependence of the resistance, the harmonics of the output voltage can be calculated from this series by applying the convolution theorem to the Fourier series. Staying within the frequency domain, the proposed method avoids numeric precision errors encountered in time-to-frequency domain transform algorithms such as Fast-Fourier-Transform [17]. First, the computation of intermodulation distortion in a shunt is presented in Section II, where the spectrum of the shunt voltage is derived and compared against simulation results.

Next, Section III covers the experimental verification, in which the distortion measurements of several shunt resistors are presented and compared to computation results. Finally, Section IV concludes the paper.

II. COMPUTATION OF INTERMODULATION DISTORTION

Most shunt resistors are specified with a worst case TCR over a given temperature range, for example 100 ppm/K from $-25\,°C$ to $125\,°C$, indicating a rise of resistance with temperature. The TCR is obtained by measuring the resistance
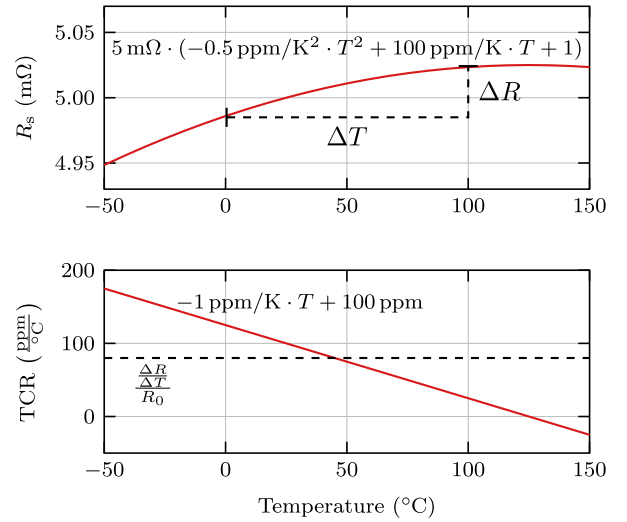

FIGURE 1. Idealized temperature dependence of a thin film 5 mΩ shunt resistor. The change of resistance per degree depends itself on the temperature.

at the beginning and end of the range, and then dividing the difference by the temperature delta [18]. Across this range, the resistance R_s of the shunt can then be expressed by

$$R_s = R_0 \cdot (1 + \alpha \cdot T_s), \qquad (1)$$

where R_0 is the resistance at a specified temperature, T_s the temperature deviation from this specified point and α the TCR. However, the resistance of a shunt depicted in Fig. 1 demonstrates that a linear approximation fails to fully describe the shunt's behavior. Due to material properties, the TCR itself varies over temperature [19]. This variation can be expressed as

$$\alpha = \alpha_1 + \alpha_2 \cdot T_s, \qquad (2)$$

with α_1 as a temperature independent and α_2 as a temperature dependent coefficient. Including this dependence in (1), yields

$$R_s = R_0 \cdot \left(1 + \alpha_1 \cdot T_s + \alpha_2 \cdot T_s^2\right). \qquad (3)$$

Given this temperature dependence, the shunt's resistance now depends on the thermal connection and the power dissipated in the shunt.

For constant power dissipation, generated by a dc current I_s, the thermal connection can be modeled as a single resistance R_{th}. The shunt temperature can then be expressed as

$$T_s = R_{th} \cdot R_s \cdot I_s^2 = R_{th} \cdot R_0 \cdot (1 + \alpha_1 \cdot T_s + \alpha_2 \cdot T_s^2) \cdot I_s^2$$

$$\Rightarrow \alpha_2 T_s^2 + \left(\alpha_1 - \frac{1}{R_{th} R_0 I_s^2}\right) \cdot T_s + 1 = 0, \qquad (4)$$

which reveals the effect of self-heating within the shunt resistor. This quadratic equation, however, is only valid for dc currents.

Alternating currents require consideration of time dependent effects in the thermal network, as the shunt can heat
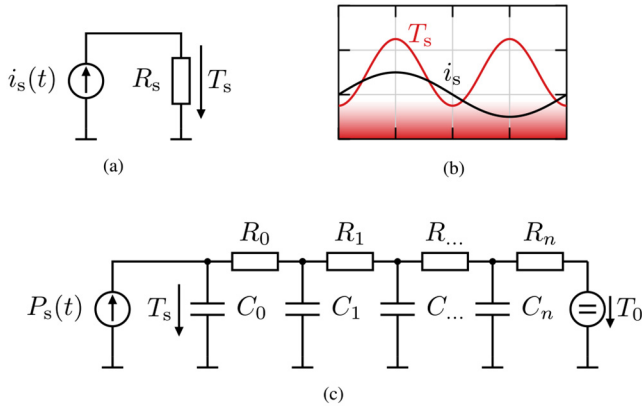
FIGURE 2. Shunt used for current sensing. (a) Electric circuit. (b) Temperature variation to load current. (c) Cauer model of the resistor's thermal network.

up or cool down within cycles. Fig. 2(a) depicts a shunt injected with an ac current of

$$i_s(t) = \hat{I}_s \cdot \sin(\omega_0 t), \tag{5}$$

with a peak value of $\hat{I}_s$ and an angular frequency of ω_0. As the power dissipation depends on the square of the current, both the positive and negative peak of i_s lead to positive peaks in the temperature, essentially creating a temperature swing with double the fundamental frequency, illustrated in Fig. 2(b). However, as the frequency increases, the temperature swing will decrease, due the thermal capacitances in the shunt. These capacitances, in combination with the thermal resistance create a low-pass filter. Fig. 2(c) shows a Cauer model which can be fitted to represent the shunt's thermal characteristic. For simplicity, a single order network is used in the presented equations, with a transfer function of

$$Z_{th}(j\omega) = \frac{R_{th}}{1 + j\omega\tau}, \qquad \tau = R_{th}C_{th}, \tag{6}$$

where C_{th} is the thermal capacitance of the shunt, as depicted in Fig. 2(c). The shunt's temperature can now be written as a convolution in the time domain as

$$T_s(t) = z_{th} * R_s(T_s(t)) \cdot i_s^2(t), \tag{7}$$

where z_{th} is the step response of the thermal network, with

$$z_{th}(t) = R_{th}e^{-t/\tau}. \tag{8}$$

Compared to the case of a dc current, the convolution in (7) makes a direct solution for ac currents difficult. However, using certain assumptions, valid approximations of the shunt temperature, and thus distortion, are obtainable.

A. DISTORTION COMPUTATION

The problem of intermodulation distortion can be simplified significantly by neglecting the influence of the TCR on the power dissipation. Assuming power dissipation independent of temperature variation, the average junction temperature over a fundamental cycle $T_{s,avg}$ can be determined by solving (4) with the rms value of $i_s(t)$.

Given the average temperature, the temperature within one cycle can be approximated by

$$T_s(t) = z_{th} * R_0 \cdot (1 + \alpha \cdot T_{s,avg}) \cdot i_s^2(t)$$
$$= z_{th} * R_0 \cdot (1 + \alpha \cdot T_{s,avg}) \cdot \frac{\hat{I}_s^2}{4}\left(-e^{j2\omega_0 t} + 2 - e^{-j2\omega_0 t}\right). \tag{9}$$

A Fourier transform of (9) and setting $\omega = n \cdot \omega_0$ yields

$$T_n \overset{\omega=n\cdot\omega_0}{=} \frac{R_{th}R_0}{1 + jn\omega_0 C_{th}R_{th}} \cdot (1 + \alpha \cdot T_{s,avg}) \cdot \frac{\hat{I}_s^2}{4}$$
$$\cdot [-\delta(n-2) + 2 \cdot \delta(n) - \delta(n+2)], \tag{10}$$

as the complex Fourier-series coefficients of T_s. The delta functions indicate that the temperature spectrum only contains a dc offset and a second harmonic component. The temperature can then be expressed in the time domain as

$$T_s(t) = \sum_{n=-\infty}^{\infty} T_n \cdot e^{j\omega_0 nt}. \tag{11}$$

Using the Fourier series of the temperature, it is possible to directly obtain the voltage spectrum across the shunt, given a sinusoidal current. The current is multiplied with the shunt resistance (3) and the temperature terms are replaced by their Fourier series, yielding (12), shown at the bottom of the page. Using the convolution theorem, the square of the junction temperature series can be expressed as a convolution with itself. For the final step, the indices inside the infinite sums are swapped between the exponential function and Fourier coefficients.

The voltage spectrum is obtained through a Fourier transform of (12), with the *nth* element equal to

$$V_n = \frac{R_0\hat{I}_s}{2j}\Big[\delta(n-1) - \delta(n+1) + \alpha_1(T_{n-1} - T_{n+1})$$
$$+ \sum_{m=-\infty}^{\infty} \alpha_2 \cdot T_m \cdot (T_{n-m-1} - T_{n-m+1})\Big], \tag{13}$$

for the complex Fourier-series coefficients of the shunt voltage. In this case, the voltage spectrum contains first, third and

$$v_s = R_0 \cdot \left[1 + \alpha_1 \cdot T_s + \alpha_2 \cdot T_s^2\right] \cdot i_s = \frac{R_0\hat{I}_s}{2j}\left(e^{j\omega_0 t} - e^{-j\omega_0 t}\right) \cdot \left[1 + \sum_{n=-\infty}^{\infty} \alpha_1 T_n \cdot e^{j\omega_0 nt} + \alpha_2 \left(\sum_{n=-\infty}^{\infty} T_n \cdot e^{j\omega_0 nt}\right)^2\right]$$
$$= \frac{R_0\hat{I}_s}{2j}\left[\left(e^{j\omega_0 t} - e^{-j\omega_0 t}\right) + \sum_{n=-\infty}^{\infty} \alpha_1 e^{j\omega_0 nt}(T_{n-1} - T_{n+1}) + \sum_{n=-\infty}^{\infty} \alpha_2 e^{j\omega_0 nt} \sum_{m=-\infty}^{\infty} T_m \cdot (T_{n-m-1} - T_{n-m+1})\right] \tag{12}$$

$$i_s = 20\,\text{A}, R_0 = 5\,\text{m}\Omega, \alpha_1 = 100\,\text{ppm}, \alpha_2 = -0.5\,\text{ppm}, R_{\text{th}} = 20\,\tfrac{\text{K}}{\text{W}}, C_{\text{th}} = 0.1\,\tfrac{\text{J}}{\text{K}}$$
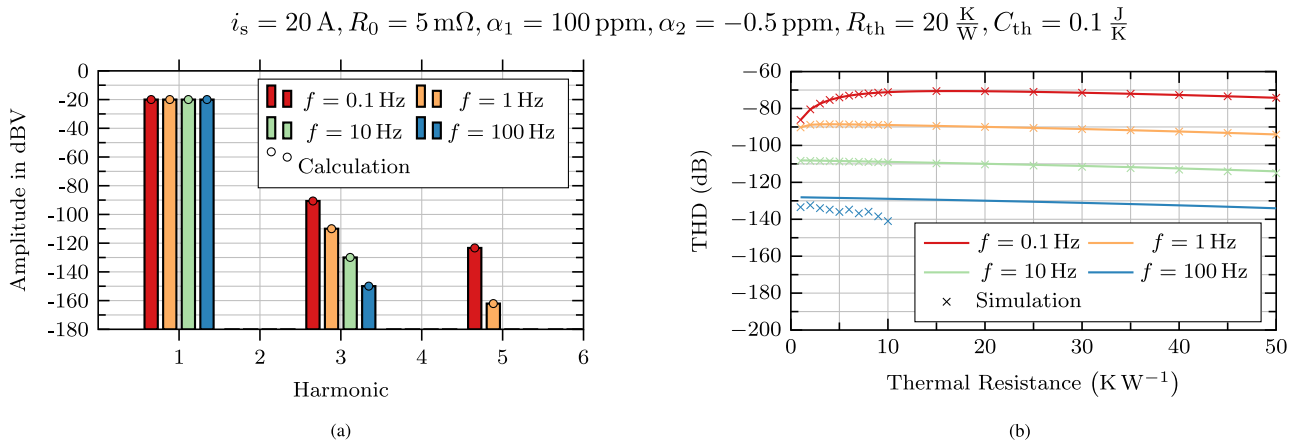

(a)

(b)

FIGURE 3. (a) Spectrum of the shunt voltage for different load frequencies obtained through simulation (bars) and computation (dots). The higher harmonics are filtered by the shunt's thermal capacitance. (b) Calculated THD of the shunt voltage over varying thermal resistance. The marks show time-based simulation results done with PLECS. The mismatch for 100Hz is attributed to PLECS' failing numerical precision at very small values.

TABLE 1. Harmonics of the shunt voltage for positive *n*.

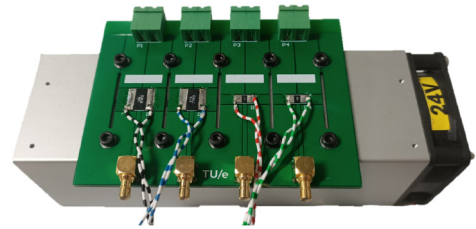| |
|---|
| $V_0 = 0$ |
| $V_1 = \frac{R_0 \hat{I}_s}{2j} \left[1 + \alpha_1 (T_0 - T_2) + \alpha_2 \left(T_0^2 + 2T_{-2}T_2 - 2T_0T_2\right)\right]$ |
| $V_2 = 0$ |
| $V_3 = \frac{R_0 \hat{I}_s}{2j} \left[\alpha_1 T_2 + \alpha_2 \left(2T_0T_2 - T_2^2\right)\right]$ |
| $V_4 = 0$ |
| $V_5 = \frac{R_0 \hat{I}_s}{2j} \alpha_2 T_2^2$ |

FIGURE 4. Test board for shunt evaluation. The board has four shunt resistors of different nominal values and different case sizes. The test current is fed through a high current connector and the shunt voltage is measured via a four point connection at the SMB coax connector.

fifth harmonic components, resulting from the dc and second order temperature components. The components for positive *n* are listed in Table 1. The components for negative *n* are the complex conjugate of their respective positive component.

Fig. 3(a) shows the voltage spectrum of a $5\,\text{m}\Omega$ shunt resistor obtained with the proposed closed-form spectral computation, compared to simulation in PLECS. PLECS is a commercial solver for dynamic and switched state-space models, able to model the time-dependent behavior of electronic components [20]. The time-intervals at which PLECS solves the system state are determined by the prescribed tolerance. At strict tolerances, required to observe low distortion levels, the simulation time increases significantly. In contrast, the closed-form spectral computation only requires to solve (13) for $n = 1, 3, 5$. The precision is determined by the utilized data type, i.e., float32 or float64. The match of closed-form spectral computation and simulation shows that the impact of temperature dependent power dissipation on the shunt's temperature is negligible. Simplification of the power losses leads to a solution with no seventh or higher harmonic, but given the low-pass behaviour of the shunt, it is guaranteed that any higher harmonic is smaller than the fifth. Furthermore, even the magnitude of the fifth harmonic is of little concern for realistic scenarios, even at very low fundamental frequencies. In fact, the fifth harmonic is can sink below the inherent thermal noise of the resistor. The thermal noise level, described in [21], is obtained through

$$v_{\text{noise}} = \sqrt{4 k_B T_s R_s f_{\text{BW}}}. \tag{14}$$

Given a sampling rate f_{BW} of 1 MHz and an ambient temperature of 300 K, the thermal noise is above the fifth harmonic for 1 Hz or higher frequencies, with a value of $-160\,\text{dB}$. Still, measuring voltages at this level would require an effective resolution of at least 26-bits, far off from any practical applications.

Fig. 3(b) shows the THD over varying thermal resistance, obtained with the proposed closed-form spectral computation. time-based simulation in PLECS. The distortion of the time-based waveforms is calculated internally in PLECS. Computation and simulation agree very well, except for a THD below $-120\,\text{dB}$. This deviation can be attributed to numeric errors due to limited precision in PLECS. Contrary to intuition, an increase in thermal resistance does not necessarily increase the THD. This behavior can be attributed to two factors. Initially one would think that an increase in thermal resistance will result in higher temperature swings, which would increase the distortion. However, a higher thermal resistance also increases the time constant of the resistor's thermal network, which dampens the temperature swing and thus reduces distortion. This effect is encapsulated in (10), as the thermal resistance R_{th} appears in the nominator but also the denominator.

The second aspect is the quadratic temperature coefficient of the resistor. Given a negative α_2, the TCR of the resistor
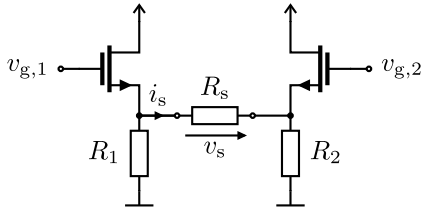
FIGURE 5. Schematic of the linear amplifier. The output current i_S is measured with a fluxgate sensor to obtain the inherent setup distortion. The voltage across the shunt resistor is expected to contain additional harmonics added through self-heating.
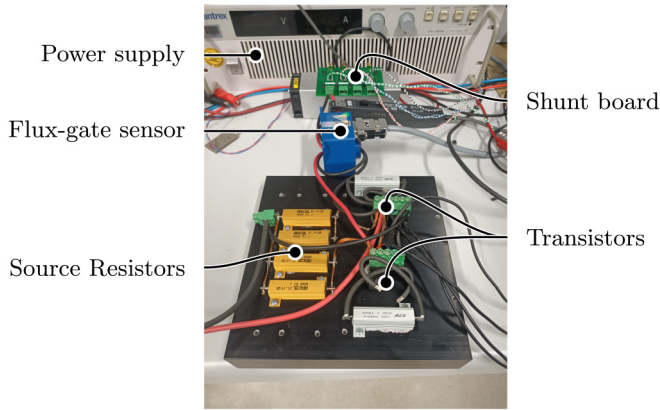

FIGURE 6. Test setup. The output of the linear amplifier is measured with a fluxgate sensor (LEM IT 60-S Ultrastab), to provide feedback for an analog PI controller (Texas Instruments OPA1612) driving the amplifier. The reference is generated by a 22-bit DAC (Applicos ATX7006A).

decreases at higher temperatures, again reducing distortion. To see whether or not the presented method is applicable, it needs to be compared against experiment results.

III. EXPERIMENTAL VERIFICATION

This section demonstrates how well the analytic solutions match with experimental observation. One problem with the verification is the low distortion of high-precision shunt resistors. As demonstrated in the previous section, a level well below -100 dB is achievable. To provide accurate measurements of the distortion caused by the shunt, the distortion of the test current must be significantly lower. Given this limit, the experiment is designed to measure shunts with a distortion of up to -80 dB. The goal is to verify the proposed computation method for varying shunt resistance, thermal resistance, thermal capacitance, and frequencies.

To cover a range of parameters, the board depicted in Fig. 4 was used. The board is populated with four shunts, each with connectors for a four point measurement. The shunts are cooled through the PCB, with the backside mounted against an over-sized heatsink. The large thermal mass of the heatsink acts as a constant temperature source and allows to simplify the shunt's thermal model. The thermal network of the shunts is modeled by a second order Cauer network, being characterized by experiment, for the two packages WSK2512 [22] and WSL3637 [23]. The distortion was measured at various frequencies, set at the current source.
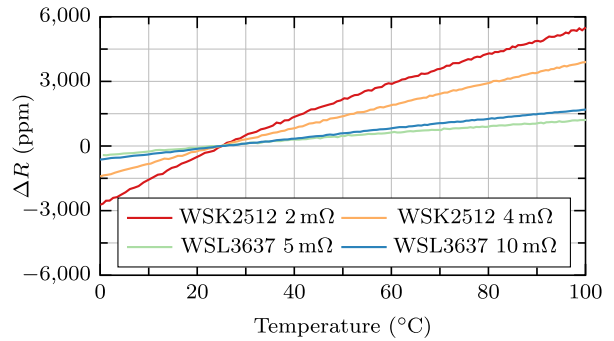

FIGURE 7. Temperature characterization of the four shunt resistors in the thermal chamber. The test current to measure the resistances is 500 mA, resulting in negligible power loss of several mW.

As stated earlier, the current source needs to have a distortion below the expected shunt distortion, as to not significantly affect the measurement. The experiment was carried out with a linear amplifier, consisting of two class A stages in a push-pull configuration, as depicted in Fig. 5. The amplifier's output current was measured with a IT 60-S Ultrastab from LEM and used as feedback for an analog PI controller, which controls the push-pull stage. The reference for the controller was generated with an Applicos ATX7006A, using the 22-bit waveform generator. The whole setup is shown in Fig. 6.

The amplifier is able to generate a 20 A sine wave with a distortion of less than -100 dB at 100 mHz. However, with increasing frequency the amplifier's distortion rises at a rate of 20 dB per decade. As the distortion across the shunts is expected to decrease with frequency, conclusive statements can be made only at low frequencies, before the amplifier's distortion and the shunt's distortion cross over. The shunt voltage was measured with the 20-bit digitizer channel of the APX2000, synchronous to the reference generation, with a noise floor below -110 dB. Prior to measuring the distortion, the thermal drift and thermal network of each shunt was identified.

First, the temperature dependence of each shunt is characterized in a thermal chamber. The chamber swept the temperature from 0 °C to 100 °C over a span of 20 minutes and the shunt temperature was monitored with a thermocouple attached to each shunt element. The resistance of the shunts was measured with a 1 A current passing through each shunt and the resulting voltage drop was measured with a twisted pair, soldered directly to each package.[1] The measurement results are depicted in Fig. 7, with the resistance normalized to room temperature. Each shunt displays a positive temperature coefficient slightly dropping of towards higher temperature, most noticeable in the 2 mΩ resistor. Each curve was fit to a second order polynomial according to (3), with the resulting coefficients listed in Table 2.

---

1. The temperature drift was initially measured through the SMB connector on the board and the observed TCR was far greater than the datasheet specification. The drift in shunt voltage seems to have been caused by an asymmetric material transition in the coaxial connector. Using a twisted pair resolved this issue.

TABLE 2. Shunt resistor characterization.

Resistor	max. TCR	R_0 (mΩ)	α_1 ($\frac{1}{K}$)	α_2 ($\frac{1}{K^2}$)
WSK2512 2 mΩ	± 250 ppm	2.008	112.3 ppm	-0.31 ppm
WSK2512 4 mΩ	± 75 ppm	4.005	58.2 ppm	-0.05 ppm
WSL3637 5 mΩ	± 50 ppm	4.976	19.6 ppm	-0.03 ppm
WSL3637 10 mΩ	± 50 ppm	9.996	28.6 ppm	-0.04 ppm
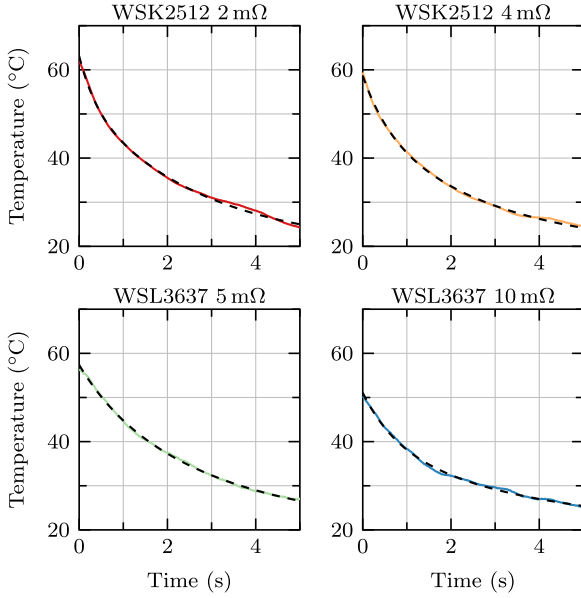
FIGURE 8. Pulse test to identify the dominant time constant of the thermal network. Measured temperature (solid line) and exponential fit (dashed).The resistors are heated with a hot air gun using a 2 mm nozzle focused on the resistive element and the resistance deviation is measured using a 1 A current, causing only insignificant power dissipation.

Given R_0 and α_1, each resistor is within specification of the datasheet regarding accuracy and drift. With the TCR determined for each resistor, the thermal network can be measured and quantified.

The resistors equivalent thermal network was obtained in two steps. First, the sum of all thermal resistances was determined by applying a dc current I_{dc} to generate the maximum rated power for each resistor and measuring the difference in resistance compared to ambient temperature. The difference in resistance was converted to a temperature difference ΔT using the polynomial fit of each shunt. The shunt's total thermal resistance was then obtained through

$$R_{th} = \frac{\Delta T}{R_s I_{dc}^2}. \tag{15}$$

The second step determines each element of the Cauer thermal network, by observing the transient thermal response to a pulsed power dissipation. To inject power, each resistor was heated with a hot-air gun, using a 2 mm nozzle focused on the resistive element.[2] The response of each shunt is depicted in Fig. 8. Using the method proposed in [24], [25], the temperature responses are used to fit a second order

2. As an alternative, the thermal step response can be observed by applying a pulsed current. However, the cables to the shunt resistor will respond to the pulse as well, creating an oscillation in the shunt voltage which can mask the voltage change due to temperature.
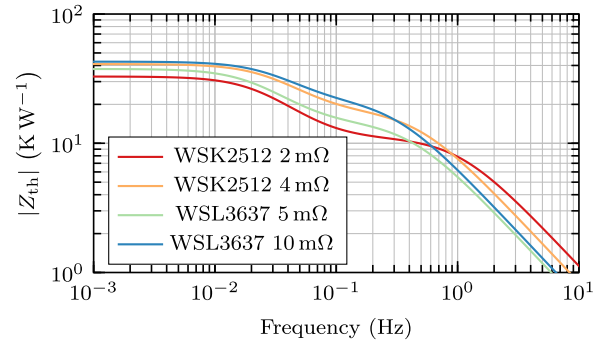
FIGURE 9. Thermal impedances extracted from the pulse test.

Cauer model to each shunt. First, the transient response is numerically fit to

$$T_s(t) - T_0 = q_0 \left(A_1 e^{-\frac{t}{\tau_1}} + A_2 e^{-\frac{t}{\tau_2}} \right), \tag{16}$$

which describes the temperature decline as a sum of two exponential functions with two different amplitudes A_1, A_2 and time constants τ_1, τ_2. The power injected by the hot-air gun q_0 is determined by dividing the peak temperature of the shunt by the previously established total thermal resistance. After the numerical calculation of all coefficients, the Fourier transfer of (16) yields the fitted thermal impedance

$$Z_s(j\omega) = R_{th} - \frac{j\omega A_1 \tau_1}{1 + j\omega\tau_1} - \frac{j\omega A_2 \tau_2}{1 + j\omega\tau_2}, \tag{17}$$

which is transformed to the thermal impedance of the Cauer network

$$Z_s(j\omega) = \frac{j\omega C_2 R_1 R_2 + R_1 + R_2}{(j\omega)^2 C_1 C_2 R_1 R_2 + j\omega(C_1(R_1 + R_2) + C_2 R_2) + 1} \tag{18}$$

All coefficients are listed in Table 3, with the detailed derivation for each coefficient listed in the Appendix. Interestingly, the resistances R_1 increase significantly with the increased nominal resistance for both package sizes. This coincides with the resistor's construction, as cuts within the element are used to obtain the nominal resistance [26]. The frequency response of each network is depicted in Fig. 9. The low frequency behavior is determined by the total thermal resistance, where the 2 mΩ resistor has the lowest impedance. At higher frequencies, the thermal capacitances come into effect, causing a -20 dB per decade roll-off. The larger internal capacitance of the WSL3637 package causes the roll-off to occur sooner for the 5 mΩ and 10 mΩ resistors, offering more damping of thermal swings at higher frequencies.

After the thermal network is identified, the distortion in each shunt is measured using the linear amplifier for a set of frequencies. The test frequencies are chosen such that the harmonics are distinct from an underlying noise at 50 Hz. In addition, one cycle of the current contains 32678 samples to improve the calculation of the spectrum. The harmonics

TABLE 3. Thermal network fit.

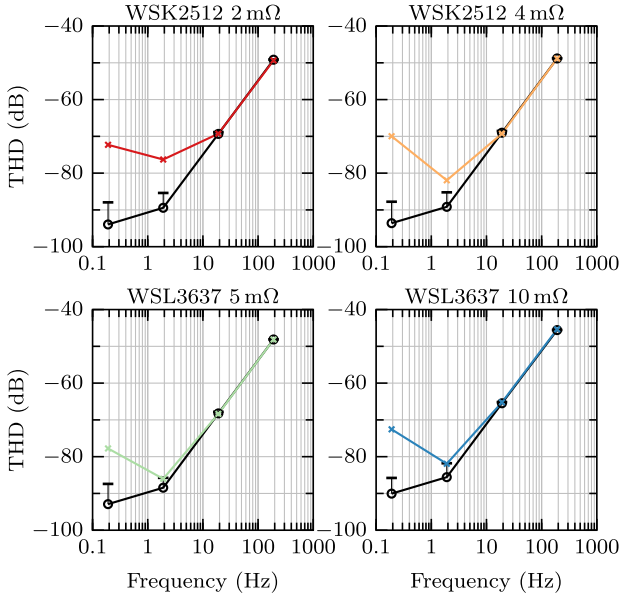| Resistor	$R_{\text{th}}\left(\frac{K}{W}\right)$	T_0 (K)	q_0 (W)	$A_1\left(\frac{K}{W}\right)$	$A_2\left(\frac{K}{W}\right)$	τ_1 (s)	τ_2 (s)	$R_1\left(\frac{K}{W}\right)$	$C_1\left(\frac{J}{K}\right)$	$R_2\left(\frac{K}{W}\right)$	$C_2\left(\frac{J}{K}\right)$
WSK2512 2 mΩ	35.07	19.68	1.32	25.19	7.65	2.72	0.37	11.47	0.0141	21.38	0.29
WSK2512 4 mΩ	38.83	19.19	0.96	29.06	11.96	2.89	0.6	19.19	0.0190	21.83	0.22
WSL3637 5 mΩ	37.26	20.3	0.99	31.41	6.17	3.12	0.89	15.73	0.0269	21.85	0.30
WSL3637 10 mΩ	41.21	20.65	0.71	27.14	15.67	3.57	0.75	23.34	0.0246	19.47	0.24

FIGURE 10. Distortion measurement of shunt current (black, circle) and voltage (color, cross). At low frequencies the shunt voltage shows an increase in THD due to intermodulation. At higher frequencies the inherent distortion of the setup becomes dominant. Error bars show worst case current distortion from sensor non-linearity of 20 ppm.

are obtained by measuring a single cycle after several seconds of continuous operation, to ensure steady-state of the thermal network. At 196 Hz, the average of ten consecutive cycles was taken. To achieve the largest possible distortion, the amplitude was set to the maximum of 20 A. Due to setup limitations, measurement at larger currents was not feasible. At lower amplitudes the effect of intermodulation distortion became difficult to observe. Furthermore, our setup illustrates the problem addressed in Section I. The controller uses the flux-gate sensor for feedback, assuming the sensor's output is the exact value of the current. However, a flux-gate sensor also contains non-linearity in its output, in this setup an error of 20 ppm full scale. Because the shape of this non-linearity is unknown, the error for the shunt voltage measurements is obtained by attributing the full non-linearity to every harmonic component. The results for each resistor are shown in Fig. 10. As indicated earlier, at low frequencies the added distortion from self-heating is evident. However, as the distortion from self-heating is expected to decrease with frequency, and the amplifier distortion increases with frequency, no observation of intermodulation distortion is possible at higher frequencies. For 196 mHz and 1.96 Hz, where the measurements are conclusive, the individual harmonics are shown in Fig. 11 and compared against results of the closed-form spectral computation as well as simulation

results. The measurements all show a pronounced third harmonic, which matches the calculation and simulation results. In contrast to the analytic solution and simulation, significant even ordered components can be seen in the shunt voltage. Their amplitude is within the possible error attributed to the fluxgate sensor, but most likely other components also contribute to the underlying noise floor. Judging from the calculation and simulation results, the fifth harmonic is too small and disappears below this noise floor. As the noise is less than the possible error, the upper error bound on the respective harmonics is more than 10 dB above the measured value. At the same time, the error could be negative enough to exactly cancel the measured amplitude, resulting in a theoretical lower error bound of $-\infty$ dB. For most of the 3rd harmonics however, the signal is large enough to have upper and lower error bounds within a few dB. At 196 mHz more conclusive statements can be made as the measurements are further above the amplifiers noise floor. The 5 mΩ has the lowest third harmonic of -78 dB, which agrees with the TCR measurements, where it showed the smallest temperature dependence of all tested resistors. In contrast, the 10 mΩ device, with only a slightly worse TCR, shows a higher harmonic of -73 dB, as the power dissipation is doubled. Between the 5 mΩ and 4 mΩ resistors, where the power dissipation is similar, the higher TCR and lower time constant of the 4 mΩ device result in a third harmonic of -71 dB. The 2 mΩ device, with even worse TCR, has nearly the same distortion at -73 dB, as it only dissipates half of the power. At 1.96 Hz, the measured distortion is higher than expected for three of the four resistors. While within the negative error bars, this is likely due to a mismatch in the thermal model. As shown in Fig. 9, the second order component of the thermal network becomes dominant before 1.96 Hz. A slight mismatch in the fitted model can result a significant change in thermal impedance at higher frequencies, and thus different results for the calculated distortion.

IV. CONCLUSION

As demonstrated in this work, the distortion in shunt resistors resulting from self-heating can be calculated accurately including non-linear effects. The results are obtained directly in the frequency domain, skipping Fourier transforms and potential numerical-precision errors. The analytic solution matches numeric simulation accurately, while computation is several orders of magnitude faster. This enables a quick search through the solution space of low-distortion current measurements. For an inverter with a specified maximum output distortion and frequency range, the closed-form spectral computation can be used to see if a specific shunt
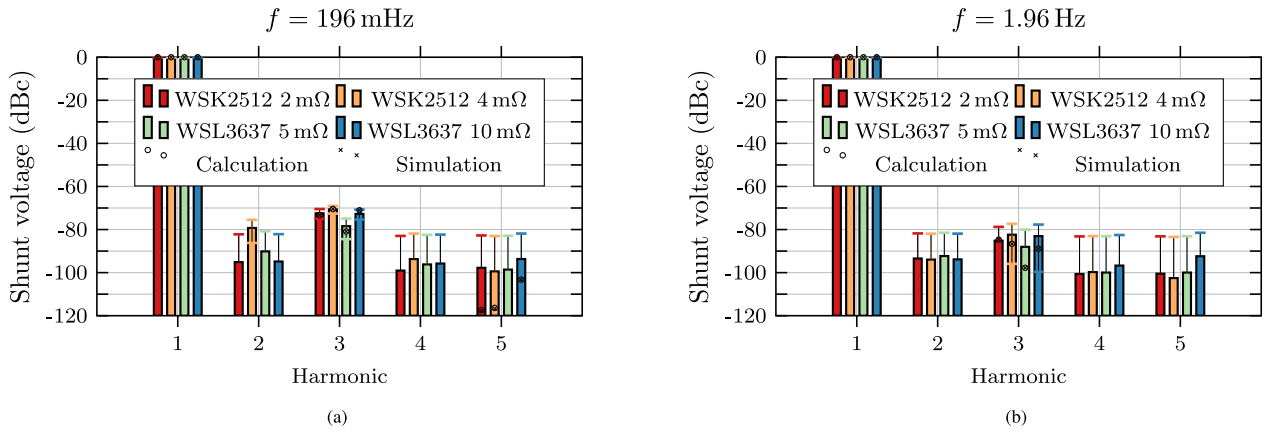
FIGURE 11. Measured voltage spectra (bars) and computations (dots) across the shunt resistors for 196 mHz (a) and 1.96 Hz (b). The third harmonic from intermodulation distortion is evident in each resistor and matches the computation in all except one case. The fifth harmonic of each shunt is likely below the noise floor of the amplifier, as indicated by the computation.

adds acceptable distortion in this range. This allows to select a component sufficient for the application, instead of over-dimensioning by choosing a shunt resistor with an extremely low TCR.

The theoretical findings are confirmed through experiments, where a linear amplifier with an output distortion of -90 dB was used to observe self-heating distortion in different shunt resistors with TCRs of 50 ppm to 250 ppm. For low frequencies, distortions of up to -70 dB are measured, matching the results from the presented computation method as well as simulation. At frequencies above 10 Hz the resistor distortion disappeared below the amplifier's noise floor. For future research, the output power of the linear amplifier could be increased, as measurements at larger output currents would show increased intermodulation distortion. In addition, the measurements could be improved by adding a low-distortion preamplifier for the shunt voltage, in order to utilize the full input range of the acquisition system. It was shown, that a larger resistor package with more thermal capacitance dampens higher harmonics and reduces distortion. Within the same package size, a lower nominal resistance experiences lower distortion due to the decreased power dissipation and lower internal thermal resistance, despite a potentially higher TCR. Furthermore, it was shown analytically that, for high frequencies, changes in thermal resistance do not affect distortion significantly. A higher thermal resistance increases the time constant of the resistor's thermal network, damping harmonics. Thus, increased cooling effort for a shunt resistor is only necessary if high dc-accuracy is required. However, knowing the TCR and thermal impedance of a shunt, accurate compensation methods exist to account for dc drift and transients [27].

APPENDIX

$$R_1 = \frac{(A_1\tau_1 + A_2\tau_2)(A_1\tau_2 + A_2\tau_1)}{A_1\tau_1^2 + A_2\tau_2^2}, \ R_2 = A_1 + A_2 - R_1 \quad (19)$$

$$C_1 = \frac{\tau_1\tau_2}{A_1\tau_1 + A_2\tau_2} \quad C_2 = \frac{\tau_1\tau_2}{R_1R_2C_1}. \quad (20)$$

REFERENCES

[1] S. Ziegler, R. C. Woodward, H. H.-C. Iu, and L. J. Borle, "Current sensing techniques: A review," *IEEE Sensors J.*, vol. 9, no. 4, pp. 354–376, Apr. 2009.

[2] S. Settels, J. Duarte, J. van Duivenbode, and C. Wijnands, "High voltage power amplifier for high precision mechatronic systems," in *Proc. 20th Eur. Conf. Power Electron. Appl. (EPE ECCE Europe)*, 2018, pp. P.1–P.10.

[3] J. A. Sabaté, R. R. Wang, F. Tao, and S. Chi, "Magnetic resonance imaging power: High-performance MVA gradient drivers," *IEEE J. Emerg. Sel. Topics Power Electron.*, vol. 4, no. 1, pp. 280–292, Mar. 2016.

[4] J. M. Schellekens, J. L. Duarte, H. Huisman, and M. A. M. Hendrix, "High-precision current control through opposed current converters," in *Proc. 14th Eur. Conf. Power Electron. Appl.*, Aug. 2011, pp. 1–10.

[5] B. Vermulst, "Baseband distortion compensation for high-precision power electronics using regularly sampled pulse-width modulators with sawtooth carrier," in *Proc. 20th Eur. Conf. Power Electron. Appl. (EPEECCE Europe)*, Sep. 2018, pp. P.1–P.6.

[6] J. M. Schellekens, J. L. Duarte, H. Huisman, and M. A. M. Hendrix, "Elimination of zero-crossing distortion for high-precision amplifiers," in *Proc. IECON 37th Annu. Conf. IEEE Ind. Electron. Soc.*, Nov. 2011, pp. 3370–3375.

[7] B. Voljc, M. Lindic, and R. Lapuh, "Direct measurement of AC current by measuring the voltage drop on the coaxial current shunt," *IEEE Trans. Instrum. Meas.*, vol. 58, no. 4, pp. 863–867, Apr. 2009.

[8] J. H. Constable, "Investigation of environmental noise in small electrical conductors," *IEEE Trans. Instrum. Meas.*, vol. 55, no. 6, pp. 2045–2054, Dec. 2006.

[9] "Using current sense resistors for accurate current measurement," Application Note e/N1702, Bourns, Riverside, CA, USA, Oct. 2008.

[10] E. Rocas, C. Collado, N. Orloff, and J. C. Booth, "Third-order intermodulation distortion due to self-heating in gold coplanar waveguides," in *Proc. IEEE MTT-S Int. Microw. Symp.*, 2010, pp. 425–428.

[11] J. Vuolevi and T. Rahkonen, "Analysis of third-order intermodulation distortion in common-emitter BJT and HBT amplifiers," *IEEE Trans. Circuits Syst. II, Analog Digit. Signal Process.*, vol. 50, no. 12, pp. 994–1001, Dec. 2003.

[12] D. Self, *Audio Power Amplifier Design*. Abingdon, U.K.: Routledge, Jul. 2013. [Online]. Available: https://www.routledge.com/Audio-Power-Amplifier-Design/Self/p/book/9780240526133

[13] E. Simon, "Resistor non-linearity—There's more to ohm than meets the eye," in *Linear Audio*, vol. 1. Scotts Valley, CA, USA: CreateSpace, Apr. 2011, pp. 138–146.

[14] J. Szwarc, "Current sensing with a precision of a few parts per million within a fraction of a second," in *Proc. IEEE Int. Conf. Microw. Commun. Antennas Electron. Syst.*, 2009, pp. 1–4.

[15] M. Mauerer and J. W. Kolar, "Distortion minimization for ultra-low THD class-D power amplifiers," *CPSS Trans. Power Electron. Appl.*, vol. 3, no. 4, pp. 324–338, Dec. 2018.

[16] M. Mauerer, "Low-noise and low-distortion switch-mode power amplifiers for nano-positioning applications," Ph.D. dissertation, Dept. Power Electron. Syst., ETH Zürich, Zürich, Switzerland, 2018, pp. 106–108.

[17] M. Tasche and H. Zeuner, "Worst and average case roundoff error analysis for FFT," *BIT Numerical Math.*, vol. 41, pp. 563–581, Jun. 2001.

[18] B. Yarborough. "Temperature Coefficient of Resistance for Current Sensing." Vishay Dale. May 2020. [Online]. Available: https://www.vishay.com/docs/30405/whitepapertcr.pdf

[19] D. W. Braudaway, "Precision resistors: A review of material characteristics, resistor design, and construction practices," *IEEE Trans. Instrum. Meas.*, vol. 48, no. 5, pp. 878–883, Oct. 1999.

[20] J. H. Alimeling and W. P. Hammer, "PLECS-piece-wise linear electrical circuit simulation for simulink," in *Proc. IEEE Int. Conf. Power Electron. Drive Syst. (PEDS)*, vol. 1, 1999, pp. 355–360.

[21] J. B. Johnson, "Thermal agitation of electricity in conductors," *Phys. Rev.*, vol. 32, pp. 97–109, Jul. 1928.

[22] "Power metal strip® resistors, low value (down to 0.0005 Ω), surface mount, 4-terminal," Data Sheet WSK2512, Vishay Dale, Columbus, NE, USA, 2022. [Online]. Available: https://www.vishay.com/docs/30108/wsk2512.pdf

[23] "Power Metal Strip® resistors, low value (down to 0.001 Ω), surface mount, 4-terminal," Data Sheet WSL3637, Vishay Dale, Columbus, NE, USA, 2022. [Online]. Available: https://www.vishay.com/docs/30099/wsl3637.pdf

[24] P. E. Bagnoli, C. Casarosa, M. Ciampi, and E. Dallago, "Thermal resistance analysis by induced transient (TRAIT) method for power electronic devices thermal characterization. I. Fundamentals and theory," *IEEE Trans. Power Electron.*, vol. 13, no. 6, pp. 1208–1219, Nov. 1998.

[25] P. E. Bagnoli, C. Casarosa, E. Dallago, and M. Nardoni, "Thermal resistance analysis by induced transient (TRAIT) method for power electronic devices thermal characterization. II. Practice and experiments," *IEEE Trans. Power Electron.*, vol. 13, no. 6, pp. 1220–1228, Nov. 1998.

[26] "12 Things to Know About Resistors in Pulse Load Applications." Vishay. 2003. [Online]. Available: https://www.vishay.com/docs/48516/_ms9702509-2003-vishaychecklistpulseload.pdf

[27] P. Weßkamp and J. Melbert, "High-accuracy current measurement with low-cost shunts by means of dynamic error correction," *J. Sens. Sens. Syst.*, vol. 5, no. 2, pp. 389–400, 2016.

PELLE WEILER (Graduate Student Member, IEEE) received the M.Sc. degree from RWTH Aachen University, Germany, in 2018. He is currently pursuing the Ph.D. degree with the Electromechanics and Power Electronics Group, Eindhoven University of Technology, The Netherlands. His main research interests include power electronics with a focus on high-precision applications, wide-bandgap semiconductors, and high-frequency magnetics.

BAS VERMULST (Member, IEEE) received the M.Sc. and Ph.D. degrees from the Eindhoven University of Technology, Eindhoven, The Netherlands, in 2012 and 2016, respectively, where he is currently an Assistant Professor with the Electromechanics and Power Electronics Group. He has also been employed for several years as an Engineer and a System Architect with high-tech industries around Eindhoven. His main research interests include power electronics and control, high-frequency switched mode power supplies, high-precision applications, and automotives.

ERIK LEMMEN received the B.Eng. degree (*cum laude*) in electrical engineering from the Fontys University of Applied Sciences, Eindhoven, The Netherlands, in 2009, and the M.Sc. and Ph.D. degrees (*cum laude*) in power electronics from the Eindhoven University of Technology, Eindhoven, in 2013 and 2017, respectively. He is currently working as a Development Engineer and a System Architect in the high-tech industry in Eindhoven, and also as a part-time Research Assistant with the Electromechanics and Power Electronics Group, Eindhoven University of Technology. His research interests include multilevel topologies, redundancy in power converters, and modular converter structures.

KORNEEL WIJNANDS (Member, IEEE) received the M.Sc. degree in electrical engineering from the Eindhoven University of Technology, Eindhoven, The Netherlands, in 1994. He joined Prodrive Technologies B.V., Son, The Netherlands, in 1994, where he started to work on the development of power electronics and control, where he is currently a Senior Electronics Architect. In 2009, he became a part-time Assistant Professor with the Electromechanics and Power Electronics Group, Eindhoven University of Technology, where he has been a Full Professor since 2017. He is currently a part-time Professor with the Electrical Energy Systems Group, Eindhoven University of Technology. His research interests include high-precision amplifiers and smart grid electronics.